LA-UR- 96-3489

CONF-9610225--1

Title: Measurement and Control of Optical Nonlinearities of Importance to Glass Laser Fusion Systems.

Author(s): N.A. Kurnit, P-24
T. Shimada, P-24
M.S. Sorem, P-24
A.J. Taylor, MST-11
G. Rodriguez, MST-11
T.S. Clement, *
D.F.V. James, T-4
P.W. Milonni, T-4

*JILA, National Bureau of Standards and Technology, Boulder, CO.

Submitted to: Second Annual Solid-State Lasers for Applications to ICF International Conference
22-25 October 1996
Paris, France

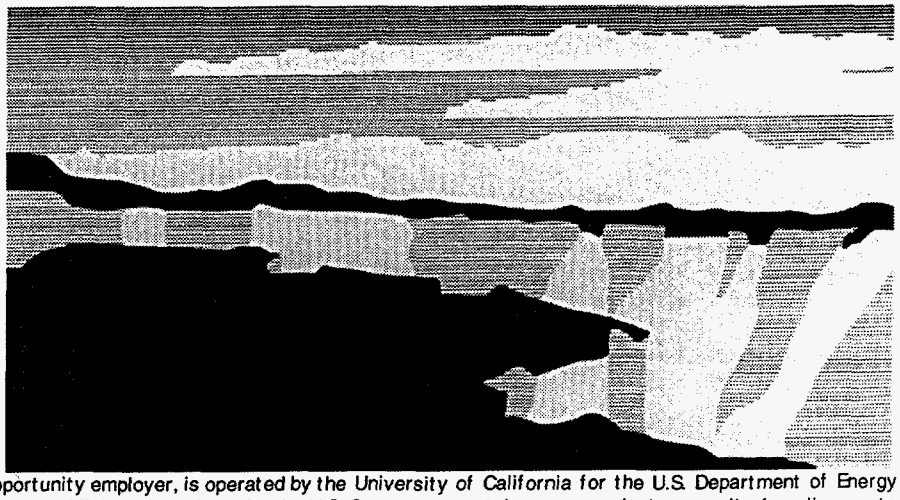

Los Alamos
NATIONAL LABORATORY

Form No. 836 R5
ST2629 10/91

DISCLAIMER

Measurement and Control of Optical Nonlinearities of Importance to Glass Laser Fusion Systems

N. A. Kurnit, T. Shimada, M. S. Sorem, A. J. Taylor, G. Rodriguez, T. S. Clement,*
D. F. V. James, and P. W. Milonni

Los Alamos National Laboratory
Los Alamos, NM 87545

ABSTRACT

Results of a number of studies carried out at Los Alamos, both experimental and theoretical, of nonlinear optical phenomena important to the design of the National Ignition Facility are sumarized. These include measurements of nonlinear index coefficients, Raman scattering in atmospheric oxygen, and theoretical studies of harmonic conversion.

Keywords: nonlinear refractive index, frequency conversion, Raman scattering

1. NONLINEAR INDEX MEASUREMENTS

Optical propagation effects due to the nonlinear index of refraction of materials, such as self-focusing and small-scale beam breakup, can be especially detrimental in high power laser systems, causing bulk damage, focusing problems, and reduced harmonic conversion efficiency. Measurements of the nonlinear index, n_2, of a number of optical materials were made to help confirm design decisions for the NIF. The motivation for this work was the relatively large scatter in data that had been obtained for fused silica by different techniques at 355 nm,[1] and the fact that filamentary bulk damage was observed in Nova target lenses at fluence levels below that anticipated for self-focusing. The measurements were made by two different techniques in order to increase confidence in the results. One method was an application of a recently-developed technique for measuring the amplitude and phase of an ultrashort pulse by "Frequency-Resolved Optical Gating" (FROG).[2-4] The other utilized a modified version of the Z-scan technique[5] that measures beam distortion introduced by scanning a sample through the focus of a beam. Our measurements by both techniques for fused silica were consistent with the lower range of previously measured values, indicating that it should not be necessary to further expand the beam size in the NIF to stay below the self-focusing threshold.

---

*Present Address: JILA, National Bureau of Standards and Technology and University of Colorado, Campus Box 440, Boulder, CO 80309

1.1 Frequency Resolved Optical Gating

FROG is a recently-developed ultrafast diagnostic technique that is currently extensively used to characterize the output of ultrafast laser systems by measuring the full electric field, both instantaneous amplitude and phase, of an ultrashort pulse in a single shot. In order to measure the nonlinear index of a material, the time-dependent phase of the pulse is compared with and without a sample of the material placed in the beam.[6] Experimentally, this technique involves splitting the pulse to be characterized into two replicas, which are then crossed in any instantaneously responding nonlinear optical medium. The signal generated by the nonlinearity is imaged onto the slit of a spectrometer and the resulting spectrogram is recorded by a two-dimensional array detector in the image plane of the spectrometer. A polarization-gate nonlinearity (with the polarization of the gate pulse rotated by 45° with respect to the pulse to be measured) has been used in these measurements because it is the simplest to interpret of a number of nonlinear geometries that can be used. Characterization of ultrashort pulses using the polarization-gating FROG geometry has been demonstrated in the visible and near infrared as well as in the uv at 308 nm.[7] The signal-pulse electric field for a polarization-gate geometry is given by $E_{signal}(t,\tau) \sim E(t)\,|E(t-\tau)|^2$, where τ is the time delay between the two pulses. The quantity $|E(t-\tau)|^2$ can be thought of as a gate that chooses a temporal slice of E(t) whose spectrum is then measured versus t. The measured signal intensity is the FROG trace, $I_{FROG}(\omega,t)$, which contains essentially all information about E(t). In order to ensure that only a uniform intensity region of this beam is sampled, a 0.5-mm slit, centered on the beam and oriented parallel to the spectrometer slit, is inserted before the cylindrical focusing lens that focuses the beams into the FROG interaction region. The problem of inverting the FROG trace to find E(t) is equivalent to the two-dimensional phase retrieval problem, a well-known, solved problem in the field of image science. We use a simple iterative Fourier transform algorithm.[2]

Measurements were made using 130 fs pulses from a Ti:Sapphire laser system at 804 nm and its second harmonic at 402 nm. The dispersion in n_2 between 1064 nm and 804 nm is expected to be relatively small and the 402 nm wavelength is sufficiently close to 355 nm that there also should not be a large difference in the values at these wavelengths. An example of intensities and phases obtained without and with a sample of fused silica in the beam are shown in Fig.1(a) and (b), respectively. Without the sample, the phase is seen to vary nearly linearly with time over the pulse and hence represents a nearly transform-limited pulse. With a 0.95-cm sample of fused silica and a peak intensity of 5.2×10^{10} W/cm^2, a much larger phase shift is imposed near the peak of the pulse. The phase shift for linear dispersion in the sample is added to the phase data with no sample present before subtracting the phases measured with and without the sample to obtain $\Delta\phi(t)$, shown in Fig. 1(c) together with the intensity profile scaled to the amplitude of the phase change.

The measured phase shift is seen to closely follow the intensity profile. This set of data yields $n_2 = 0.85 \times 10^{-13}$ esu. The average of a number of measurements with different intensities and sample lengths is given in Table 1. The uncertainty in the measurement is dominated by uncertainty in the fluence measurement rather than uncertainty in the phase measurement. Measurements of cross-phase modulation between 804 nm and 402 nm are currently in progress.

A related technique that utilizes spectral analysis of a short pulse before and after propagation through a nonlinear medium of known nonlinear index[8] has recently also been used to measure n_2.[9] They obtain a value of $n_2 = 0.98 \pm 0.10 \times 10^{-13}$ esu for Suprasil compared to an apparently assumed value of $1.11 \pm 0.08 \times 10^{-13}$ esu for Herasil. We have attempted to use this technique and find that we do not get the same pulsewidth results as with FROG. There are also some questions on the convergence of this technique to a unique solution.[10]

1.2 Z-scan measurements

Our measurements with the Z-scan technique utilized both the original gaussian beam method[5] and a top-hat method[11] with a modification discussed below. In the gaussian beam Z-scan method, one focuses as good an approximation to a TEM_{oo} gaussian beam as one can achieve into a sample that is scanned through the focal region of the beam. An aperture is centered on the beam well beyond the focus, and the energy that passes through the aperture is recorded as a function of the distance of the sample from the focus. When the sample is far from the focus, the intensity is low and the beam is undistorted. As the sample is brought toward the focus (from the direction of the focusing lens), a positive nonlinearity will focus the beam a little tighter, increasing the size of the beam at the aperture, and decreasing the energy through the aperture. The energy through the aperture reaches a minimum when the sample is centered at $0.86\ z_o$ from the focus, where z_o is the confocal parameter, and returns to its initial value when the sample is at the focus. On the other side of focus, it acts to concentrate the energy through the aperture, reaching a peak at $0.86\ z_o$ and then returning to its initial value. The amplitude of this dispersion-shaped curve can be related to the magnitude of n_2.[5] It was shown in Ref. 11 that if one uses a circular flat-top beam as the input instead of a gaussian, the amplitude of the Z-scan curve is actually 2.5 times as large for the same peak focal intensity. This has the further advantage that one can in principal achieve a high-quality flat-top beam by greatly expanding the beam (provided enough energy is available) and selecting a small circular area near the center. It is not always possible to assure that one has a perfect gaussian beam, particularly after a harmonic conversion process, which leads to some uncertainty in relating the measured Z-scan curve to the nonlinear index. We have demonstrated, however, that the deviation from the gaussian result is not large if one has a reasonably good gaussian beam, and have obtained good agreement between the two techniques at 1064 nm by taking into account a small amount of astigmatism in the gaussian beam, resulting in a 9% correction to the gaussian result.[12] Our measurements at 355 nm were carried out only with the top-hat technique.

Our top-hat measurement technique, as shown in Fig. 2, differed somewhat from that in

Ref. 11 in that we chose to place the defining aperture for the top hat at the front focal plane of the focusing lens, and used a second lens to relay image this aperture onto a ccd camera, which was used to record the whole image rather than only measuring the energy through an aperture. A ccd was likewise used to record the data for the gaussian case. We believe there are several advantages to this relay-imaging technique. In the absence of relay imaging the beam incident on the detector shows strong Fresnel diffraction fringes, whereas it is a smooth distibution with well-defined edges in the case of relay imaging. Furthermore, if there is any wedge in the sample, the beam moves across the detector without relay imaging (which would greatly affect data taken with a fixed aperture), but remains stationary with relay imaging. The use of a ccd camera for recording the data allows one to check for spurious effects such as interference fringes (originating from the sample or lenses) moving across the image, or for changes in input beam distibution. An example of data taken by this technique is shown in Fig. 3.

The values of n_2 obtained for a number of materials by the FROG and Z-scan technique are given in Tables I and II respectively, and the values for fused silica are plotted in Fig 4, together with the results presented in Ref. 1 and some other recent determinations. The curves shown in Fig. 4 were calculated in Ref. 1 based upon a perturbation theory analysis (solid curve) and a Kramers-Kronig analysis based upon an effective two-photon resonance. Both models predict a relatively small increase out to 3ω. It should be noted that the absolute value of the curves have been arbitrarily chosen to pass through the point $n_2 = 0.95 \times 10^{-13}$ esu at 1ω; this value cannot be predicted by existing theories with any accuracy. The preponderance of more recent data appears to suggest that a value closer to 0.85×10^{-13} esu would be more appropriate. The 804-nm FROG results are consistent with earlier measurements of fused silica near 1 μm, whereas the Z-scan results presented in Table II are about 15% lower.[13] Another set of comparably low Z-scan results for fused silica, including results at second, third, and fourth harmonics, has recently been reported[14] and is included in Fig. 4. We do not know whether there is some reason for Z-scan measurements to give consistently low values compared to other techniques. The major uncertainty in our Z-scan measurement is believed to result from the determination of the pulse shape, particularly the amount of energy in the tail, which affects both the peak intensity and the fraction of the energy that has its focus changed. The pulses, which were generated from a Q-switched single-mode pulse by means of a Pockels cell driven by a 500-ps pulse from an avalanche transistor driver, unfortunately did have substantial energy in a low-level tail as discussed in more detail in Ref. 12. The pulses were measured on a 60-ps-risetime Hamamatsu photodiode and Tektronix 7250 6-GHz oscilloscope at 1064 nm and 355 nm and by a streak camera at 355 nm.. These photodiodes are known to exhibit a non-negligible tail when excited by a short pulse and it was subsequently confirmed at 355 nm that the photodiode signal exhibited a somewhat larger tail than the streak camera. Applying the same correction for the pulse shape at 1064-nm as measured at 355 nm resulted in a reduction of approximately 11% in the 1064-nm n_2 values from those obtained with the pulse shape recorded by the photodiode. The error limits largely reflect this uncertainty in the pulse

shape factor, together with a relatively small allowance for the uncertainty in energy and spot size, as well as an allowance for the consistency of the individual data sets in yielding a precise peak-to-valley ratio. This latter factor is generally smaller than the uncertainty introduced by the pulse shape, except for some data from poorer samples such as fast growth KDP and older KD*P, where some irreproducible absorption features were observed during 355-nm scans. We believe this was probably due to two-photon absorbing inclusions, since similar behaviour was not observed at 1064 nm. This is an area where we believe some followup work may be necessary in order to characterize samples of NIF-grade materials.

Several different types of fused silica were measured by the Z-scan technique, including Corning 7940 and 7980, Suprasil II, Dynasil 1000, and a sample of fused quartz from the French laser program. No statiscally significant differences were measured for different samples, so only an average value is quoted in Table II. Measurements on KDP labeled (o) and (e) were made with the light wave polarized perpendicular and parallel to the optic axis, respectively. Both the FROG and Z-scan measurements yielded values for the (o) polarized wave consistently higher than for (e) polarized wave. The value labeled (oe) for KD*P is actually for an (e) wave, but one that is polarized at an angle to the optic axis, as this crystal was cut for doubling and the beam could not be propagated with its polarization parallel to the optic axis.

Laser glasses were measured in the same range as previous measurements,[15-17] with LG-770 measuring slightly lower than LHG-8 and LG-750.

1.3 Other sources of self-focusing

These measurements indicate that self focusing due to n_2 in KDP or fused silica are not large enough to be responsible for filamentation observed in Nova target lenses. Another n_2-like effect that has been examined as a possible source of phase perturbations that can initiate filamentation in downstream optics is related to the harmonic generation process itself.[18] With a second-harmonic crystal detuned from perfect phase matching, as is the case in the baseline design, Ref. 18 shows that there is an intensity-dependent phase shift imprinted on the fundamental. This would show up as a phase imprinted on the third harmonic in the tripler. However, numerical calculations with the code discussed in the next section indicate that this may be a contributing factor, but is not as significant a potential problem as the effect of the spatially varying phase in the input beam discussed below, and is in any case is included in the calculation.

2. Optimization of third-harmonic generation and control of phase perturbations

Previously reported work carried out in collaboration with LLNL personnel, principally J. M. Auerbach and D. Eimerl, has been directed toward the development of improved frequency converters for the frequency tripling of 1053 nm laser radiation.[19-22] Predictions of the codes

that were developed have been found to be in very good agreement with experimental data obtained at LLNL over the past few years. Aside from providing accurate simulations of existing experimental data, this collaborative effort has evaluated a number of possible "advanced" converter designs for efficient high-dynamic range and/or large-bandwidth conversion. These designs involve three or four crystals instead of the NIF baseline design employing two crystals, i.e., a single doubler and a single tripler. High dynamic range designs are useful not only for increasing the efficiency of conversion of shaped pulses, but also for providing high conversion efficiency if the fundamental drive intensity must be limited for some reason, e.g. by Raman scattering as discussed in the next section.

One of the most significant outcomes of this work is the identification of the importance of spatial phase variations across the 1053-nm pump radiation. This recognition came as a result of the detailed computer simulations carried out to compare theory to experiment, and led to further analytical studies as well as experimental studies at LLNL.[20-22] The latter have corroborated the main code predictions and the underlying theory of the role of "phase ripples" in high-power frequency conversion.

It also appears that spatially varying phase (as well as intensity) in the fundamental may be responsible for significantly enhanced phase and intensity variation in the third harmonic field that could be the cause of the damage observed in Nova target lenses. The multiple-crystal designs that provide high-dynamic range efficient[20] conversion also appear to have some advantage in mitigating this problem compared to the baseline design. This is illustrated in Fig. 5, which shows the fundamental input containing phase and intensity ripples and third-harmonic output profiles for the (a) baseline design of a 1.1-cm doubler detuned by 250 μrad and an aligned 0.9-cm tripler, and (b) a 3-crystal design that has been shown to give high efficiency over a broad dynamic range, consisting of a 1.3-cm doubler detuned by 385 μrad and a 1.0-cm doubler detuned by -494 μrad, followed by the same 0.9-cm tripler. The ripples have been imposed in the same way as was experimentally studied,[21,22] namely by adding a weak reflection from two surfaces of a fused silica wedge. However, they could be caused by diffraction from machining grooves on the KDP, or by propagation of phase perturbations from earlier in the system.

The baseline design is seen to produce intensity ripples in the output that are more than twice as large as the input. The 3-crystal design gives an increase of only about 30% in the ripple intensity, while increasing the conversion efficiency to 89.4% from the baseline efficiency of 83.7% (for an assumed super-gaussian pulse in space and time). Another case has been found (two 1.5-cm doublers detuned by ±324 μrad and the same tripler) that reduces the output ripple amplitude by a factor of two compared to the pump, but at the expense of a drop in efficiency to 69.9%. An even more dramatic decrease in ripple intensity has been found for a much lower input intensity case that was being investigated for a possible experiment to study these effects with a commercial Nd:YAG laser. In this case, shown in Fig. 5 (c), there are two KD*P 1.6-cm doublers detuned by ± 150 μrad, followed by a 1.5-cm KD*P tripler. The ripple amplitude on the third harmonic is seen to be greatly reduced, but the

efficiency of 55.2% is somewhat below the 60-70% efficiency calculated for nearby designs that produced worse ripple. This example provides some reason to believe that there may be other designs possible for the NIF and LMJ that can produce reasonable efficiency with decreased phase and amplitude variations. We have not as yet uncovered any systematic way of finding such solutions, but are hopeful that a pattern will begin to emerge from a sufficient number of trial and error cases.

3. Raman gain in air and breathable mixtures

Stimulated rotational Raman scattering in nitrogen in the long paths required to bring a beam to target has been a concern for laser fusion because of the degradation to beam quality and harmonic conversion efficency that results from generation of off-axis radiation.[23] The solution originally proposed for the NIF to avoid this problem was to place part of the beam path in a breathable argon/oxygen mixture in order to reduce the path length in nitrogen below threshold level. This is desirable for safety reasons as opposed to using beam tubes containing an inert gas such as He or argon. Unfortunately, some earlier calculations,[24] and experiments performed to verify them[25] indicate that the peak Raman gain in oxygen is approximately 77% that of nitrogen (or even a few percent higher). This implies that one can only increase the threshold by 25 to 30% by replacing part of the air path with a breathable argon/oxygen mixture.

The calculation of the rotational Raman gain for O_2 proceeds along the same lines as that for N_2, with some minor complications due to the fact that the ground state of O_2 is a spin triplet. The existence of the fine structure caused by the triplet nature of the rotational levels turns out to only have a small effect, because the spliiting for the lines of interest is only $\sim\pm 0.02$ cm^{-1} about line center, well within the pressure-broadened linewidth at atmospheric pressure. This splitting reduces the peak gain by typically 15%. The surprisingly large gain for oxygen despite the nearly 1:4 population ratio in air results from a larger polarizability anisotropy, giving a 2.5 times larger Raman cross section, a slightly higher population in each level because of the absence of even levels, and a slightly smaller pressure-broadening coefficient. A stick spectrum of the calculated gain is shown in Fig. 6. It is interesting to note that there is some near overlap between lines of oxygen and nitogen, and we believe that this may be responsible for the observation of a line previously attributed to the weak S(9) of nitrogen[26] but more likely due to S(13) of oxygen or to the overlap of the two.

The relative gain of nitrogen and oxygen was measured at 355 nm by focusing ~270 mJ through a focus in air and then through a focus in a cell that could be filled with different gas mixtures. Most of the data was taken with a double pass of this arrangement, although threshold could be reached in a single pass. Attempts to perform similar measurements at 1064 nm failed because of breakdown at the focus. However, calculations indicate that the ratio of peak oxygen to nitrogen gain should only change from 77% to 79% in going from 1064 nm to

355 nm. The input beam was circularly polarized to prevent on-axis gain suppression by Stokes-anti-Stokes coupling, which is important for a focused beam in a medium with low dispersion.

By placing a mixture of 20% O_2/80% Ar in the cell, the observed spectrum was that of oxygen rather than nitrogen. With this mixture diluted by approximately 50% air, it was possible to obtain spectra in which the lines of both nitrogen and oxygen had approximately the same threshold, as shown in Fig.7, which also shows the calculated stick spectrum for this mixture. It is interesting to note that the overlapped S(13) of O_2 and S(9) of N_2 is the strongest line of the spectrum in these cases, and is probably enhanced by running the laser broadband in one case. From the ratios of pressures of the two gases in the different parts of the path when the gains were equalized, together with the measured transmission losses, it is possible to calculate a ratio of the peak gain of O_2 to N_2 of 81±2%, compared to the 79% calculated at this wavelength. The major uncertainty in the calculation is the lack of a measured value for the broadening coefficient of oxygen by nitrogen, which can easily account for the small difference in measured and calculated values. The calculated ratio at 1053 nm is 77%; this would yield a threshold improvement of 30% if a sufficient pathlength in air were converted to O_2/Ar to avoid scattering in nitrogen. The actual improvement to be expected might be a few percent less if one extrapolates the 1053-nm gain ratio to 79% based on the measured value at 355 nm.

In order to try to mitigate this problem, we are beginning to look calculationally at the effect of smoothing by spectral dispersion (SSD) on the Raman threshold. This was shown to have some benefit experimentally in Ref. 25. We would like to be able to quantify just how much threshold improvement one can obtain in this way. We will also be looking at what effect, if any, the broadband amplifed spontaneous emission from the laser chain might have on reducing the threshold

References

1. R. Adair, L. L. Chase, and S. A. Payne, "Dispersion of the nonlinear index of optical crystals," Optical Materials **1**, 185 (1992).
2. D. J. Kane and R. Trebino, "Characterization of arbitrary femtosecond pulses using frequency-resolved optical gating" IEEE J. Quantum Electron. **29**, 571, (1993).
3. R. Trebino and D. J. Kane, "Using phase retrieval to measure the intensity and phase of ultrashort pulses: frequency-resolve optical gating," J. Opt. Soc. Am. A, **10**, 1101 (1993)
4. T. S. Clement, A. J. Taylor, and D. J. Kane, "Single shot measurement of the amplitude and phase of ultrashort laser pulses in the violet," Opt. Lett **20**, 70 (1995) and references therein.
5. M. Sheik-Bahae, A. A. Said, T. H. Wei, D. J. Hagan, and E. W. Van Stryland, "Sensitive measurements of optical nonlinearities using a single beam," IEEE J.

Quantum Electron. **26**, 760 (1990).

6. A. J. Taylor, G. Rodriguez, and T. S. Clement, "Measurement of n_2 for KDP and fused silica at 800 nm and 400nm," Opt. Lett. to be published.
7. D. J. Kane, A. J. Taylor, R. Trebino, and K. W. DeLong, "Single-shot measurement of the intensity and phase of a femtosecond UV laser pulse with frequency-resolved optical gating," Opt. Lett. **19**, 1062 (1994).
8. B. S. Prade, J. M. Schins, E. T. Nibbering, M. A. Franco, and A. Mysyrowicz, "A simple method for determination of the intensity and phase of ultrashort optical pulses, Opt. Commun. **113**, 79 (1994).
9. E. T. Nibbering, M. A. Franco, B. S. Prade, G. Grillon, C. LeBlanc, and A. Mysyrowicz, "Measurement of the nonlinear refractive index of transparent materials by spectral analysis after nonlinear propagation," Opt. Commun. **119**, 479 (1995).
10. E. T. Nibbering, M. A. Franco, B. S. Prade, G. Grillon, J.-P. Chambaret, and A. Mysyrowicz, "Spectral determination of the amplitude and phase of intense ultrashort optical pulses," J. Opt. Soc. Am. B **13**, 317 (1996).
11. W. Zhao and P. Palffey-Muhorey, "Z-scan technique for top-hat beams," Appl. Phys. Lett. **63**, 1613 (1993).
12. T. Shimada, N. A. Kurnit and M. Sheik-Bahae, "Measurements of nonlinear index by a relay-imaged top-hat Z-scan technique," *Laser-Induced Damage in Optical Materials: 1995* (Proceedings of the 27th Annual Boulder Damage Symposium, Oct. 30-Nov. 1, 1995, Boulder, CO), SPIE Vol.2714, p. 52.
13. The results presented in Ref.12 are quoted as even lower, by an additional 7%, owing to an even larger correction assumed at the time. Some problems identified with streak camera uniformity and calibration have prompted us to use a smaller correction.
14. R. DeSalvo, A. A. Said, D. J. Hagan, E. W. Van Stryland, and M. Sheik-Bahae, "Infrared to ultraviolet measurements of Two-photon absorption and n_2 in wide bandgap solids," IEEE. J. Quantum Electron. **32**, 1324 (1996).
15. D. Milam and M. J. Weber, "Nonlinear refractive index coefficient for Nd phosphate laser glasses," IEEE J. Quantum Electron. **12**, 512 (1976).
16. M. J. Weber, D. Milam, and W. L. Smith, "Nonlinear refractive index of glasses and crystals," Opt. Eng. **17**, 463 (1978)
17. A. N. Azarenkov, G. B. Al'tshuler, N. R. Belashenkov, and S. A. Kozlov, "Fast nonlinearity of the refractive index of solid-state dielectric active media" (review), Quantum Electron. **23**, 633 (1993).
18. R. DeSalvo, D. J. Hagan, M. Sheik-Bahae, G. Stegeman, and E. W. Van Stryland, "Self-focusing and self-defocusing by cascaded second-order effects in KTP," Opt. Lett. **17**, 28 (1992).
19. D. Eimerl, J. M. Auerbach and P. W. Milonni, "Paraxial wave theory of second and third harmonic generation in uniaxial crystals," J. Modern Optics **43**, 1037 (1995).

20. P. W. Milonni, J. M. Auerbach, and D. Eimerl, "Frequency conversion modelingwith spatially and temporally varying beams," *Proceedings of the First Annual Conference on Solid State Laers for Application to Inertial Confinement Fusion,* Montery, CA. May 31-Jun 2, 1995, SPIE Vol.2633, p.230.
21. J. M. Auerbach, D. Eimerl, J. T. Hunt, D. Milam, J. B. Trenholme, and P. W. Milonni, "Perturbation theory for frequency doubling and tripling of electric field amplitude and phase ripples," ibid, p. 655.
22. J. M. Auerbach, D. Eimerl, D. Milam, and P. W. Milonni, "A perturbation theory for electric field amplitude and phase transfer in frequency doubling and tripling," Appl. Opt. to be published.
23. M. A. Henesian, C. D. Swift, and J. R. Murray, "Stimulated rotational Raman scattering in nitrogen in long air paths," Opt. Lett. **10**, 565 (1985).
24. N. A. Kurnit, "Rotational Raman Gain of Atmospheric O_2," Fourth International Laser Science Conference (ILS-IV), Atlanta, GA, October 2-6, 1988, paper WE-5, Bull. Am. Phys. Soc. 33, 1651 (1988).
25. N. A. Kurnit, "Calculation and measurement of stimulated rotational Raman scattering in atmospheric oxygen," Conference on Lasers and Electro-Optics (CLEO'96), Anaheim, CA, June 2-7, 1996, paper CThK57, (OSA 1996 Technical Digest, Vol.9, p. 434.), and in preparation.
26. M. D. Skeldon and R. Bahr, "Stimulated rotational Raman scattering in air with a high-power broadband laser," Opt. Lett. 16, 366 (1991).

Table I

Measured n_2 values obtained by Frequency-Resolved Optical Gating

(in units of 10^{-13} esu)

	λ = 804 nm	λ = 402 nm
Fused silica	0.86 ± 0.08	1.14 ± 0.13
KDP (o)	1.05 ± 0.11	1.48 ± 0.18
KDP (e)	0.96 ± 0.09	1.43 ± 0.17

Table II

Measured values of γ and corresponding n_2 obtained by Z-scan techniques

	n_o	γ (10^{-16} cm^2/W)	n_2(10^{-13} esu)	
1064 nm:				
Fused silica	1.45	2.07±0.4	0.72±0.13	(near top-hat)
		2.10±0.4	0.73±0.13	(gaussian)
LHG-8	1.52	3.15±0.5	1.15±0.19	(near top-hat)
LG-750	1.52	3.16±0.5	1.15±0.19	(near top-hat)
LG-770	1.52	2.90±0.5	1.06±0.18	(near top-hat)
		3.35±0.7	1.22±0.23	(gaussian)
BK-7	1.51	2.41±0.5	0.87±0.16	(near top-hat)
KDP(e)	1.46	2.50±0.5	0.88±0.16	(near top-hat)
KDP(o)	1.49	2.78±0.5	0.99±0.19	(near top-hat)
		2.75±0.5	0.98±0.19	(gaussian)
KD*P(o)	1.46	3.18±0.6	1.11±0.22	(near top-hat)
		3.20±0.6	1.12±0.22	(gaussian)
KD*P(oe)	1.47	2.84±0.5	1.00±0.18	(near top-hat)
KBr	1.54	6.36±1.4	2.35±0.50	(gaussian)
355 nm				
Fused silica	1.47	2.74±0.4	0.97±0.15	(top-hat)
KDP(e)	1.49	5.00±0.8	1.79±0.30	(top-hat)
KDP(o)	1.53	5.90±1	2.16±0.35	(top-hat)
KD*P(o)	1.53	8.35±1.5	3.06±0.55	(top-hat)
KD*P(oe)	1.50	6.06±1	2.18±0.35	(top-hat)

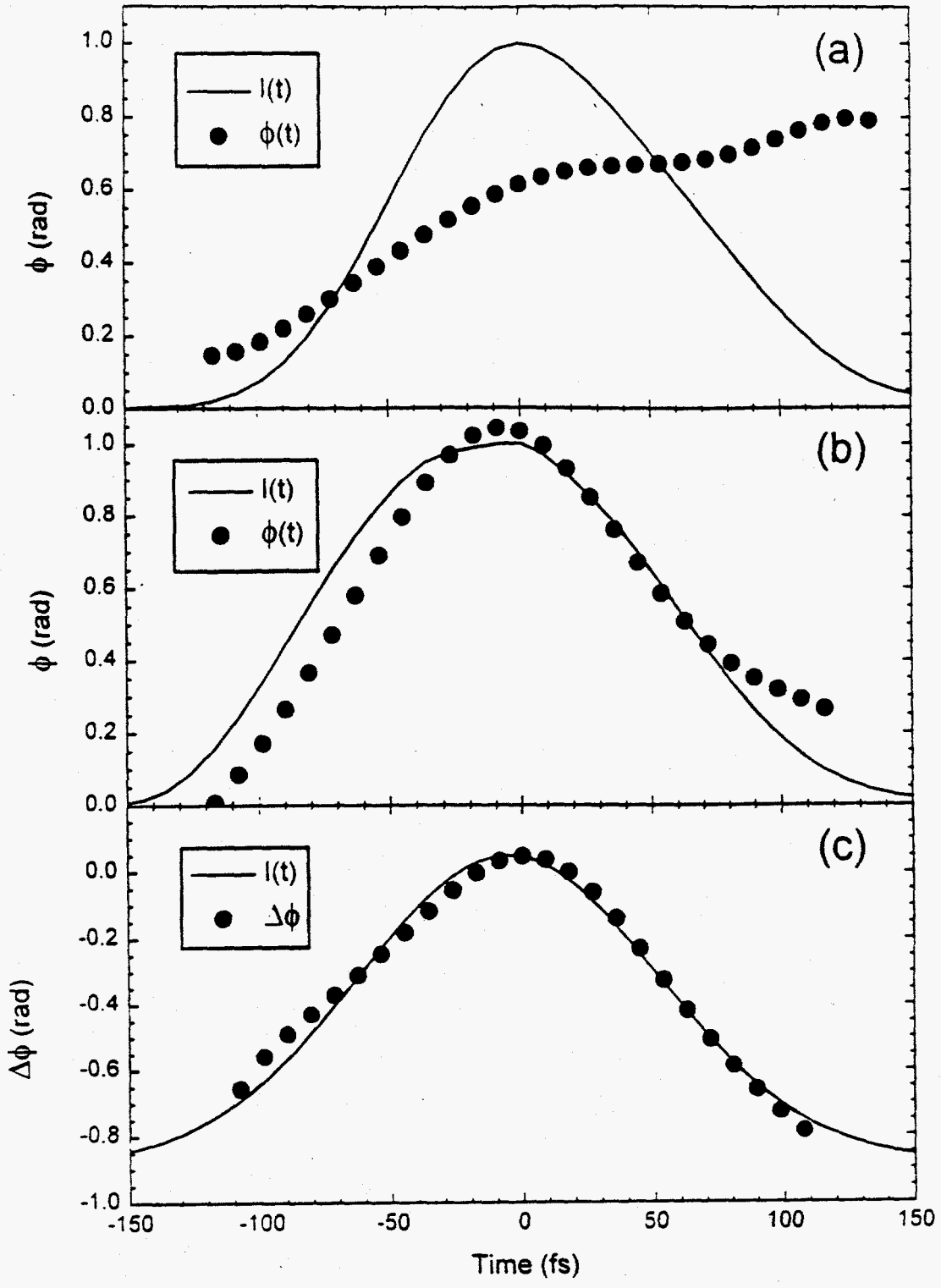

Fig.1 FROG data showing intensity any phase a) without sample, b) with sample, and c) phase difference with intensity curve normalized to peak phase shift.

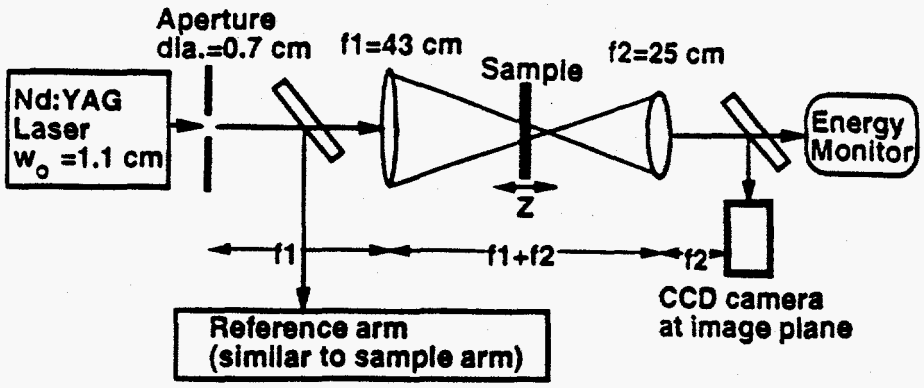

Fig. 2. Experimental setup for relay-imaged top-hat Z-scan at 1064 nm. The defining aperture for the top hat is placed at the front focal plane of the focusing lens and imaged onto the ccd camera by a second lens.

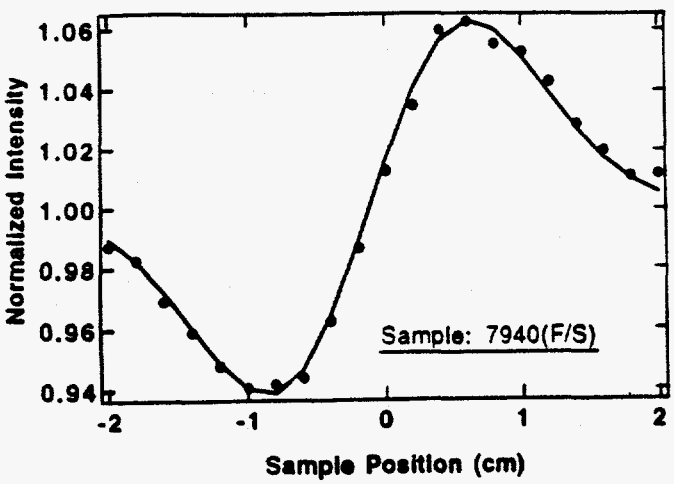

Fig. 3. Fit of Z-scan data for fused silica obtained with a near top-hat truncated gaussian at 1064 nm to the derivative of a gaussian.

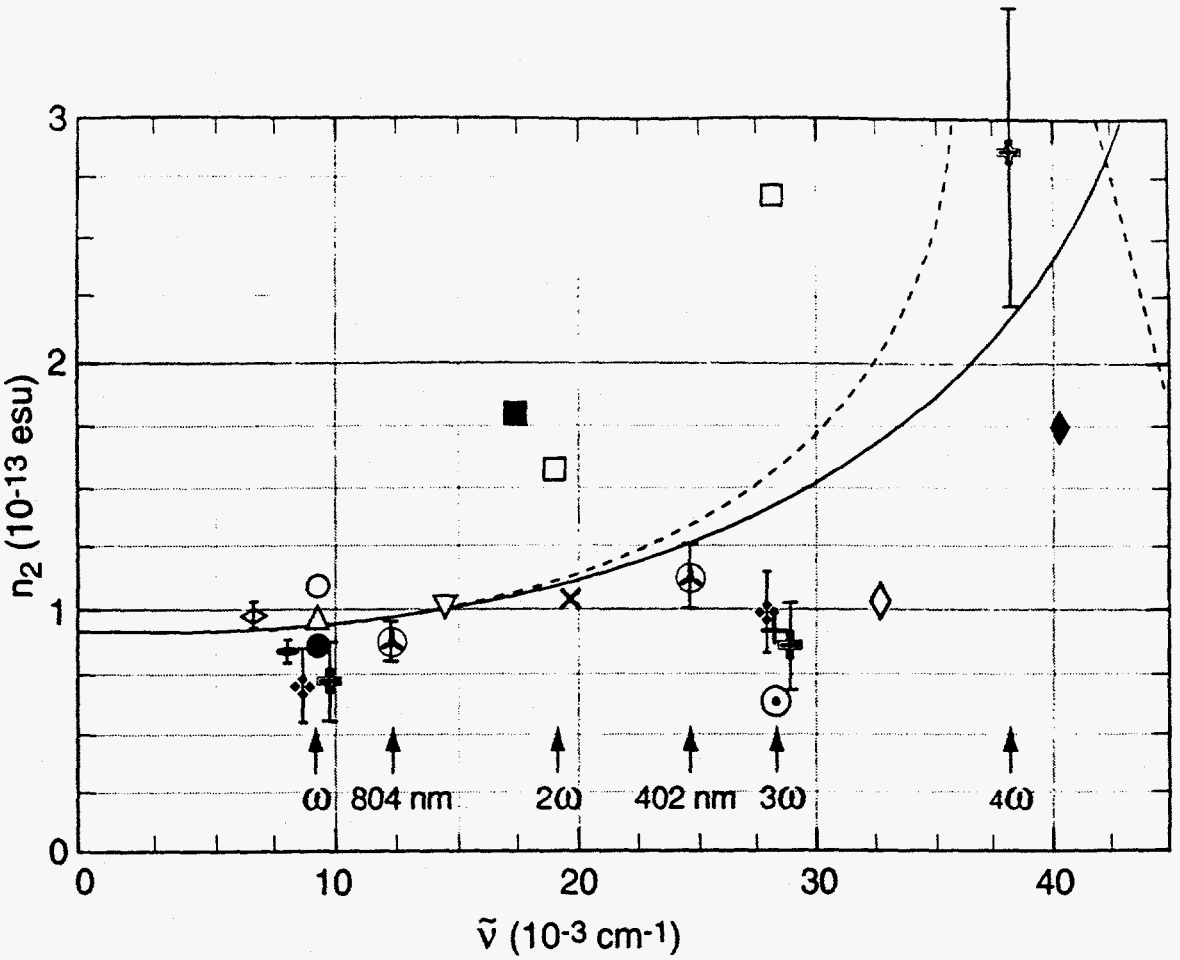

Fig. 4. Compilation of fused silica n_2 data from Fig. 6 in Ref. 1, redrawn (with minor corrections) and updated with our data and other recent measurements (points for which error bars are shown). Theoretical curves were obtained in Ref. 1 from a perturbation theory analysis (solid) and a Kramers-Kronig analysis (dashed). Added points are displaced horizontally at 1ω and 3ω for clarity.

△ D. Milam and M. J. Weber, J. Appl. Phys. **47**, 2497 (1976)

○ K. B. Altshuler et al., Sov. Tech. Phys. Lett. **3**, 213 (1977)

● R. Adair, L. L. Chase, and S. A. Payne, J. Opt. Soc. Am. B **4**, 875 (1987)

▽ A. Owyoung, IEEE J. Quantum Electron. **QE-9**, 1064 (1973)

× R. H. Stolen and C. Lin, Phys. Rev. A **17**, 1448 (1978), corrected in Opt. Lett. **19**, 257 (1994)

■ M. D. Levenson, IEEE J. Quantum Electron. **QE-10**, 110 (1974)

□ R. Adair, L. L. Chase, and S. A. Payne, Opt. Materials **1**, 185 (1992) (Ref. 1)

◇ Y. P. Kim and M. H. R. Hutchinson, Appl. Phys. B **49**, 469 (1989)

♦ I. N. Ross et al., J. Mod. Optics **37**, 555 (1990)

⊙ W. L. Smith et al., Conf. on Lasers and Electro-Optics, CLEO '83, paper FB-4

+ W. T. White III, W. L. Smith and D. Milam, Opt. Lett. **9**, 10 (1984)

A. J. Taylor, T. S. Clement, and G. Rodriguez, LANL FROG measurements

❖ T. Shimada and N. A. Kurnit, LANL Z-scan measurements

✙ R. DeSalvo et al., CREOL Z-scan measurements, IEEE J. Quantum Electron. **32**, 1324 (1996)

◇ T. Kato et al., Opt. Lett. **20**, 988 (1995) cross-phase-modulation in fibers at 1.55 μm

– K. S. Kim et al., Opt. Lett. **19**, 257 (1994), self modulation in fibers at 1.319 μm

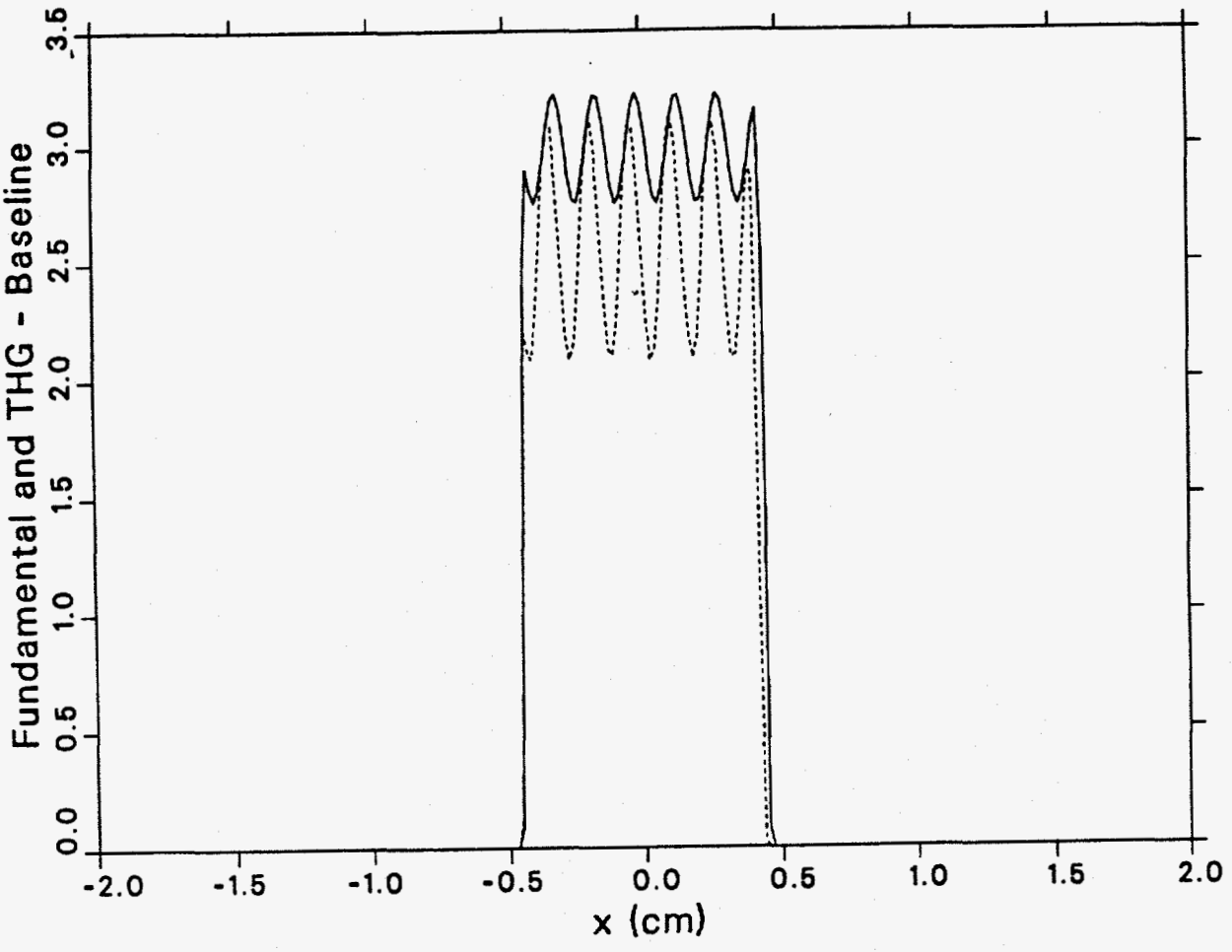

Fig. 5(a). Fundamental input (solid) and third harmonic output (dashed) for baseline case of 1.1-cm doubler detuned by 250 μrad and an aligned 0.9-cm tripler.

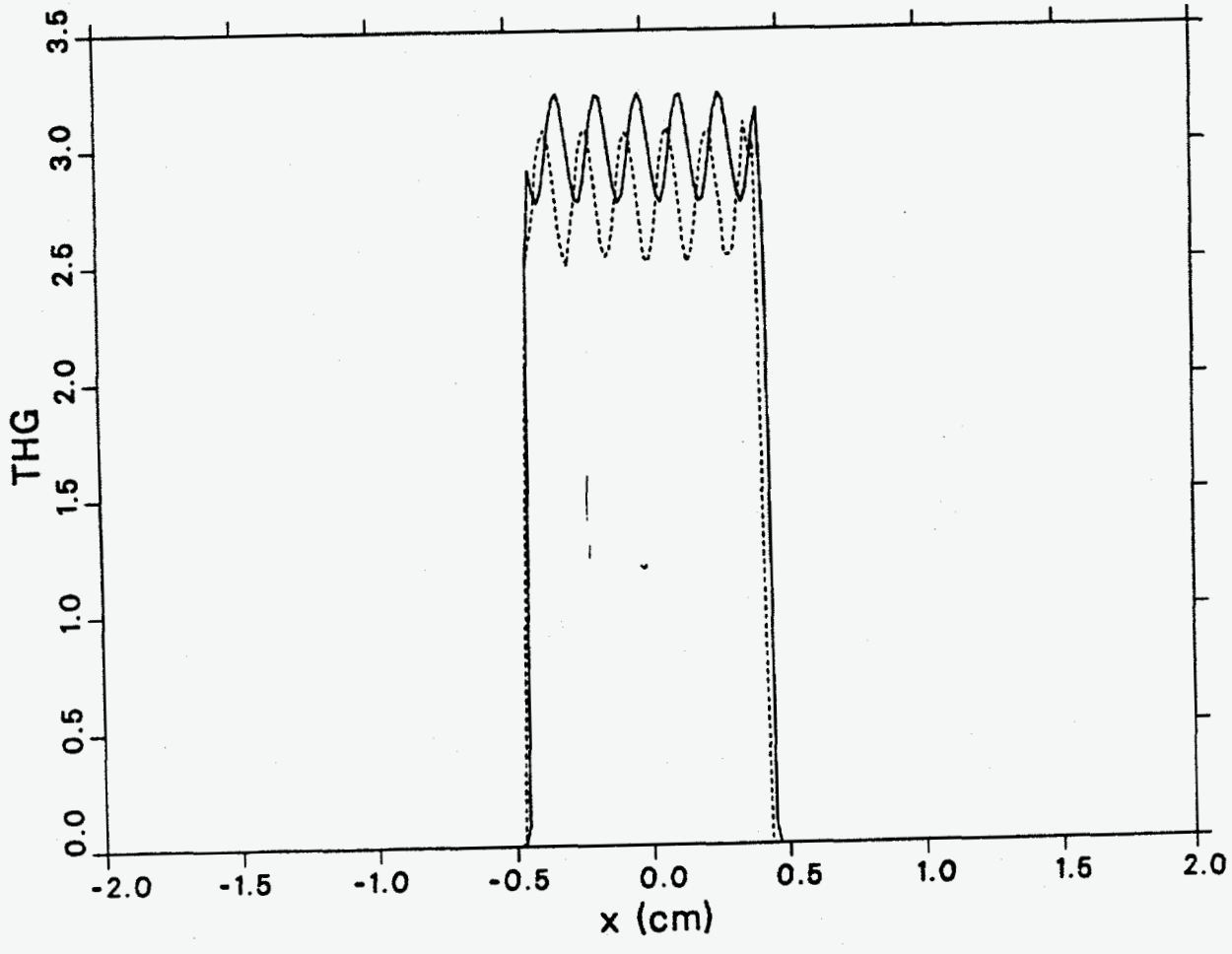

Fig. 5(b) Fundamental input (solid) and third harmonic output (dashed) for a 3-crystal design consisting of a 1.3-cm doubler detuned by 385 μrad, a 1.0-cm doubler detuned by -494 μrad, and an aligned 0.9-cm tripler.

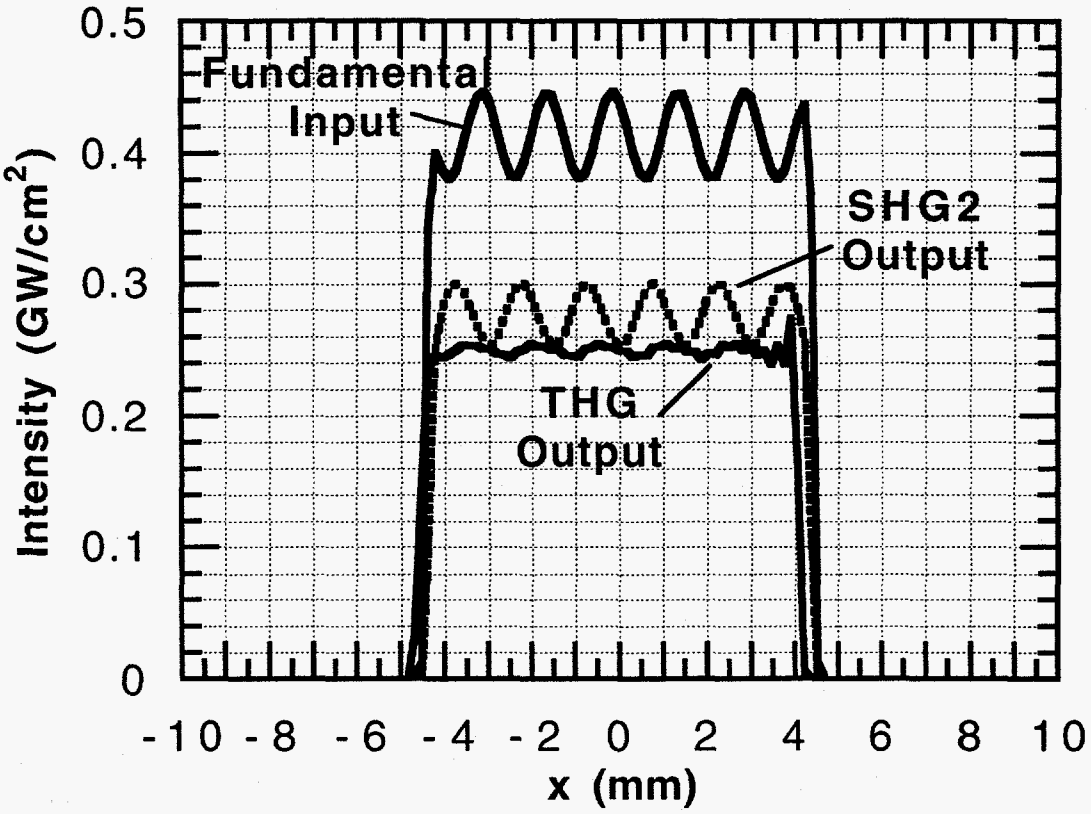

Fig. 5(c). Fundamental input, output of second SHG crystal, and third harmonic output for low intensity case with two 1.6-cm doublers detuned ±150 μrad and single 1.5-cm tripler.

Fig. 6 Raman Gain in Air at 295 K for 1053-nm Pump

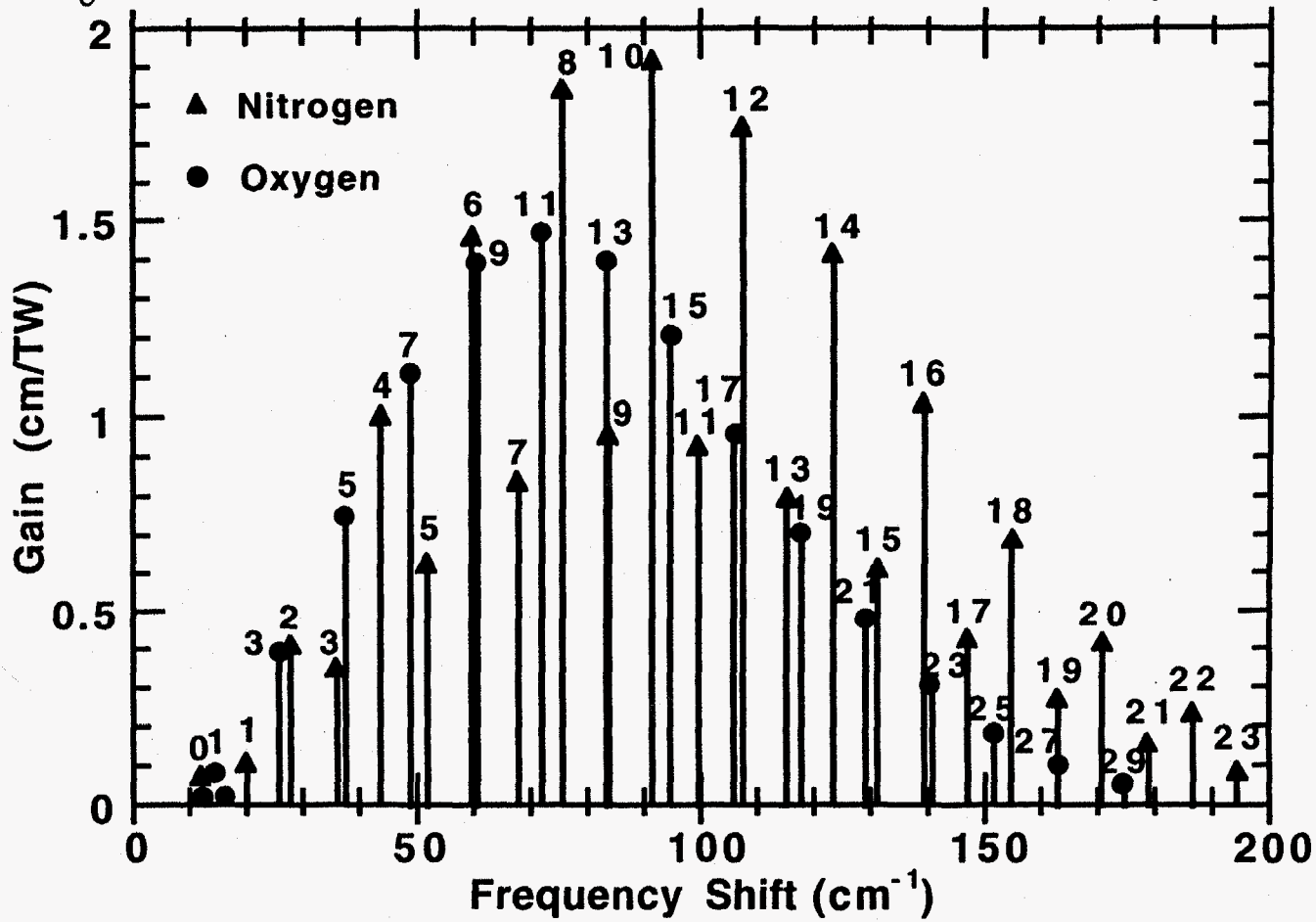

Fig. 7 **Spectra With Gas Mixtures In Cell**